MECHANISMS TO ARREST A CRACK IN THE ADHESIVE BONDLINE OF FATIGUE LOADED CFRP-JOINTS USING A RIVETLESS NUTPLATE JOINT

R. Sachse[1], A.K. Pickett[1] , M. Gnädinger[1], P. Middendorf [1]

[1]Institute of Aircraft Design, University of Stuttgart, Pfaffenwaldring 31, 70569 Stuttgart, Germany
Email: sachse@ifb.uni-stuttgart.de, Web Page: http://www.ifb.uni-stuttgart.de/mitarbeiter/sachse.html

Keywords: Fatigue simulation, adhesive bonding, hybrid composite joints, crack growth, crack arresting

Abstract
Adhesively bonded composite joint configurations with different mechanical fasteners were investigate to identify and quantify mechanisms that arrest crack growth in the adhesive bondline when loaded in fatigue. A screening test program of three different joint configurations, consisting of the rivetless nut plate joint, a pin and a bolt configuration, under three different load levels was performed. A numerical fatigue model was implemented in the finite element code ABAQUS to numerically predict fatigue crack growth and was shown to correspond well with experimental results and is able to predict the change of loading in the adhesive. The test results show a significant crack growth reduction at all load levels particularly for the rivetless nut plate joint. Using the simulation peeling load reduction due to the mechanical fastener was identified as the leading mechanism to arrest crach growth. Further local reinforcement through bearing load transfer is also required for effective crack arrest.

1. Introduction

The increased application of carbon fiber reinforced plastics (CFRP) in the aerospace industry has led to a demand for joining methods that consider lightweight design philosophies with corresponding predictive analysis tools. Adhesive bonding is considered a promising alternative to commonly used mechanical fasteners. Their application to primary aircraft structures, however, is restricted by current aerospace certification regulations because undetectable weakbonds can evolve and propagate as a crack under realistic high cycle fatigue loading. According to AC20-107B [1] a combination of adhesive bonding with mechanical fastening must therefore be used. Following a “no growth” certification approach that is currently the industry standard, a large amount of fasteners must be used so that any initial debonds cannot grow. This results in a significant weight penalty for these joints. [1, 2, 3]. In contrast to this conventional approach, research currently pursued within the EU funded FP7 project BOPACS [2] aims to design “damage tolerant” composite joints. While initial cracks can occur locally due to weak bonds, alternative features shall be used to arrest fatigue crack growth before it becomes critical. This approach requires a thorough understanding of crack arresting features and load transfer mechanisms as well as predictive tools for the joint design.

The behavior of fatigue loaded adhesive joints has been widely studied. It has been shown [3] that even at a fraction of its static untimate strength fatigue cracks can grow at a significant rate. A dominating factor influencing the crack growth rate was identified to be the mode of loading where cracks can grow in pure mode I loading several orders of magnitude faster than in mode II loading [4, 5]. Real aerospace structures experience a combination of mode I and mode II loading. Consequently, the Cracked Lap Shear (CLS) specimen has been successfully used to approximate the low load transfer of joints such as

Excerpt from ISBN 978-3-00-053387-7

stringer-skin connection [6] and was therefore adopted for work presented here. Improvements in fatigue life of bonded joints have been demonstrated through the application of mechanical fasteners. Lin et al. [7] have shown that interlaminar crack growth can be arrested under static loading in CLS-specimen using bolts. More recently, Sachse et al. [6] have demonstrated the crack arresting capabilities of a rivetless nut plate joint and several pin configurations in fatigue loaded bonded CLS-specimens. These studies suggest that the primary crack arresting mechanisms are suppression of peeling mode stresses and local reinforcements. A quantification of the different mechanisms has not been provided to date.

The prediction of fatigue crack growth in adhesively bonded joints is a central question for design of damage tolerant joints. Several models have been developed in Finite Element (FE) codes using cohesive zone elements, where static damage variables have been extended to capture fatigue damage evolution by linking damage mechanics to an experimentally determined Paris' Law curve. Conventional models rely on a global cohesive zone length parameter to compute local damage rate at each integration point. This cohesive zone length in turn depends on the specimen geometry and loading condition and therefore prevents a general application of these models to more complex three-dimensional structures [8, 9].

Based on a method by Kawashita et al. [10], Sachse et al. [11] have recently presented the implementation of a fatigue model capable of predicting arbitrary crack growth in adhesively bonded joints using a crack tip degradation approach. The model has been successfully applied to predict the influence of a rivetless nutplate joint on crack propagation in a bonded CLS specimen under fatigue loading. This paper presents a more detailed analysis, both experimentally and numerically, on the mechanisms acting to arrest a crack in the adhesive bondline. Starting from a rivetless nut plate joint, two further configurations of crack arresting features separately studying local reinforcement and suppression of peeling mode stresses are being investigated. Additionally, the effect of different load levels on behaviour of the rivetless nut plate joint is presented. Numerical simulations are then used to capture and quantify parameters that cannot be measured experimentally.

2. Static and Fatigue Model

The simulation of fatigue crack growth is modelled by applying a load or displacement envelope, instead of modelling each cycle individually (see Figure 1). First, the model is loaded to a maximum fatigue load, then cohesive zone elements are used to extract the applied strain energy release rate which is used during a subsequent fatigue step. A static and fatigue constitutive model for an 8-node three-dimensional cohesive zone element (CZE) has been implemented in the commercial software ABAQUS using a user-defined material subroutine for explicit time-integration (VUMAT). For quasi-static loading, a standard bi-linear cohesive zone approach (Eq. 1) correlating traction t to the element stiffness K and displacement δ has been used. A quadratic interaction criterion for damage initiation (Eq. 2) with traction t^0 at damage initiation and a power law criterion (Eq. 3) with the critical strain energy release rate G_c and the fitting factor α to described mixed-mode propagation has also been implemented.

$$t_i = \begin{cases} (1 - D_{static}) K_i \, \delta_i; \delta_I, \delta_{II} \geq 0 \\ K_I \, \delta_I; \delta_I \leq 0 \end{cases} \quad (1)$$

$$\left(\frac{\langle t_I \rangle}{t_I^0}\right)^2 + \left(\frac{t_{II}}{t_{II}^0}\right)^2 = 1 \quad (2)$$

$$\left(\frac{G_I}{G_{IC}}\right)^\alpha + \left(\frac{G_{II}}{G_{IIC}}\right)^\alpha = 1 \quad (3)$$

where subscripts I, II in Equations 1-3 represent mode I and mode II loading respectively.

The fatigue model extends static damage variable D_{static} by a fatigue damage variable leading to a total damage evolution $\dot{D}_{tot} = \dot{D}_{static} + \dot{D}_{fatigue}$. Fatigue damage evolution is described through the Paris'

Excerpt from ISBN 978-3-00-053387-7

Law (Eq. 4) which correlates strain energy release rate amplitude ΔG to crack growth rate da/dN using the fitting parameters C_1 and C_2. These fitting parameters are again a function of the mixed mode ratio $MMR = G_{II}/(G_I + G_{II})$, (Eq. 5). Using a crack tip degradation approach, where only elements in the crack front experience fatigue degradation, the Paris' Law can be expressed in terms of fatigue damage evolution $dD_{fatigue}/dN$ by assuming the remaining damage at the beginning of fatigue degradation $(1 - D_{static})$ is accumulated once the crack has passed through the element with an effective length l_e (Eq. 6). In order to relate fatigue damage to the number of cycles N, a numerical fatigue frequency f_{num} is introduced (Eq.7). During each time step Δt, the cohesive zone element is therefore damaged according to a certain block of cycles ΔN defined by the numerical fatigue frequency (Eq. 8).

$$da/_{dN} = C_1 \Delta G^{C_2} \tag{4}$$

$$C_j(MMR) = MMR \cdot C_{j_I} + (1 - MMR) \cdot C_{j_{II}} \; ; j = 1{,}2 \tag{5}$$

$$\frac{dD_{fatigue}}{dN} = \frac{1 - D_{static}}{\Delta N_e} = (1 - D_{static}) \frac{da}{dN} \, l_e \tag{6}$$

$$f_{num} = \frac{dN}{dt} = \frac{\Delta N_e}{n_{\Delta t_{fail}} \Delta t} \tag{7}$$

$$D_{fatigue}^{t} = D_{fatigue}^{t-1} + \frac{dD_{fatige}}{dN} \cdot f_{num} \cdot \Delta t \tag{8}$$

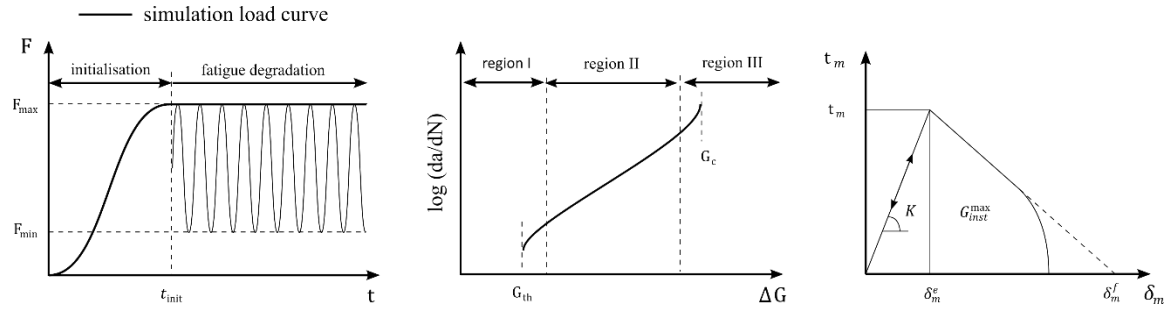

Figure 1: Load envelope (left), Paris' law curve (center), modified traction separation law (right) [11]

3. Test Specimen Design and Test Setup

3.1. Test Specimen Design

The CLS specimen has been selected as a suitable joint geometry to investigate crack arresting capabilities of a bonded-rivetless nut plate joint (RNPJ). Preliminary simulations have shown that in a load controlled fatigue test with a constant R-ratio and maximum fatigue load, the CLS specimen provides a section of constant strain energy release rate (ΔG) and mixed mode ratio (MMR) resulting in a constant crack growth rate. This makes it particularly suited for investigation of crack arresting features. Figure 2 shows a schematic drawing of the test specimen. The 2mm thick adherents are made of Hexply IM7/8552 UD prepreg featuring a quasi-isotropic layup with a stacking sequence of [0°, 45°, 90°, −45°]$_s$. A Teflon foil has been added during the bonding process to achieve an artificial pre-crack. The RNPJ is installed in the middle of the 40mm wide specimen at a distance of 45mm from the pre-crack. This leaves a region of about 45mm for undisturbed crack growth behind the RNPJ. The laminate was cured according to the manufactures specifications. In order to ensure a reproducible surface quality, the fluoropolymer release film (Airtech WL5200) was applied to both sides. Prior to bonding, the surface was cleaned with isopropanol and low pressure plasma surface treated to remove a significant amount

Excerpt from ISBN 978-3-00-053387-7

of fluorine remains coming from the release film. The toughened epoxy-based adhesive (Scotch-Weld 9323 B/A) was selected for this study and cured at 65°C for 2hrs. The bondline thickness was controlled by two precision thickness gauge strips with a thickness of 0.5mm placed along each side of the plate; loading tabs were then bonded to the cured joint and the final test specimen was cut using a precision diamond saw.

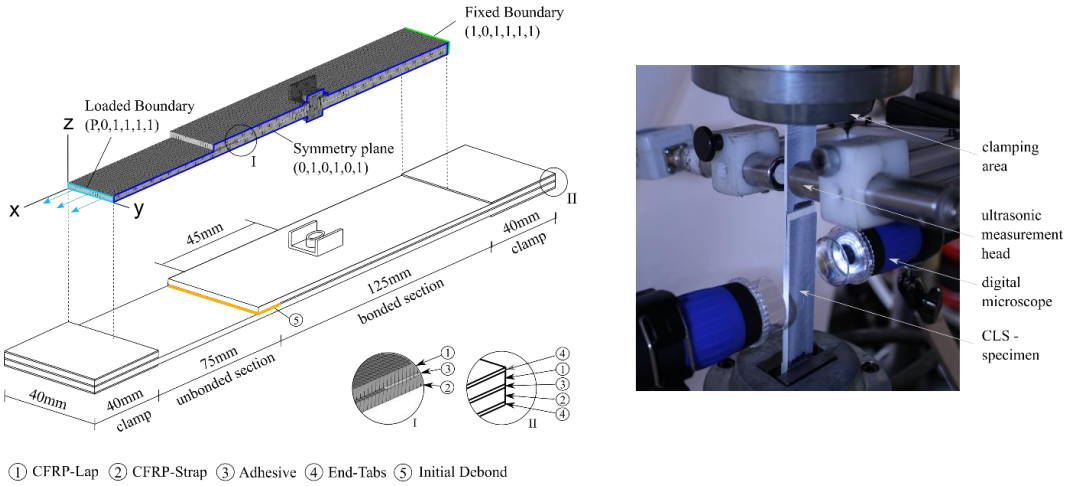

Figure 2: Schemetic drawing and numerical model of the CLS specimen (left) with test set up (right)

3.2. Test Setup

Fatigue tests were performed on a 25kN IST and 250kN INSTRON servo-hydraulic testing machine with the following parameters for the load controlled constant amplitude fatigue test:

- **R-ratio** = 0.1
- **Frequency, f** = 5 Hz
- **Maximum Fatigue load,** $\boldsymbol{F_{max}}$: 14kN, 20kN, 30kN

As shown in Figure 2, two measurement systems have been integrated into the test machine to allow an in-situ measurement of the crack length. Two USB camera microscopes were also used on each side of the specimen. By painting the side faces white a better contrast was achieved. This system is comparitively easy to evaluate and works well with mode I loading. Disadvantages do, however, arise when pure mode II loading acts at the adhesive making it very difficult to visually determine the crack front. It also provides only a one-dimensional resolution of the crack front. In order to measure the two-dimensional crack growth, an additional automated air-coupled ultrasonic measurement system was found necessary and integrated into the test rig. Results presented in this paper will focus only on visual inspection.

3.3. Discussion of Crack Arresting Features

The rivetless nut plate CNP53C3-1-03 by Cherry® [12], which is specifically designed for composite materials in combination with a MS983-11 bolt, was selected as baseline for these studies. The rivetless nut plate consists of a nut plate retainer that is pressed in to the composite prior to bonding and a floating nut. Due to clearance between the bolt and the retainer, manufacturing tolerances can be compensated allowing a separate drilling prior to assembly. The installation procedure on a laboratory scale has been defined in such a way that this clearance is filled with adhesive to ensure an optimal load transfer. Figure 3 shows a microsection of the installed RNPJ.
From inspection of the assembly cross-section in Figure 3, the following crack arresting mechanisms can be postulated:

- Local reinforcement through the mechanical joint and subsequent reduction of ΔG_{tot} acting at the adhesive *(Bolt-Composite Interface, Bolt-Sleeve Interface)*

Excerpt from ISBN 978-3-00-053387-7

- Suppression of mode I loading in the adhesive *(Nut Plate/Washer-Composite Interface)*

The effect of local reinforcement and suppression of mode I loading is investigated in detail. Figure 3 presents a schematic illustration of the additional configurations investigated:

1. **Pin Configuration (PC):** The bolt is replaced by a pin, but still integrated into the rivetless nut plate as defined for the RNPJ. Due to the missing head, peel load transfer into the pin is significantly reduced, ideally limiting it to a pure bearing load transfer.
2. **Bolt Configuration (BC):** During fabrication process of the RNPJ adhesive is prevented from flowing into the clearance between bolt and retainer limiting it to a pure mode I load transfer.

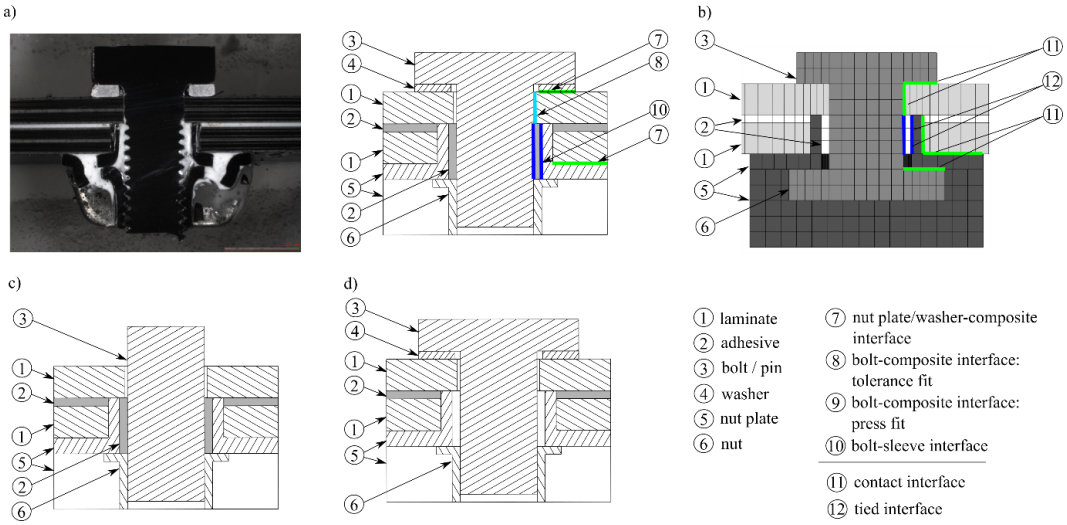

Figure 3: Crack arresting features a) rivetless nut plate joint b) numerical model of rivetless nut plate joint c) pin coniguration d) bolt configuration

4. Results

An experimental screening test program was carried out to investigate the three different configurations of crack arresting features discussed in section 3.3 at a maximum load level of 20kN (**RNPJ20kN** - rivetless nut plate joint, **PC20kN** – pin configuration, **BC20kN** – bolt configuration) . Additionally the rivetless nut plate joint configuration was tested at 14kN and 30kN (**RNPJ14kN, RNPJ30kN**). A minimum of two test specimens per configuration and load level were made. The mean crack length measured from both specimen sides will be presented here. Due to variations of the initial crack growth rate, a direct comparison is difficult. It was therefore decided to present the crack length with respect to the normalized fatigue cycle, which is normalized by the fatigue cycles required to reach a crack length of 45mm, representing the average initial crack growth rate, (Eq 9).

$$cycle_{norm} = \frac{cycle}{cycle_{@\ a=45mm}} \tag{9}$$

Numerical simulations were conducted corresponding to each test specimen configuration and load level. Figure 2 shows the numerical model of the CLS specimen with a RNPJ including defined boundary conditions. Continuum shell elements were used for the composite adherents with the corresponding stacking sequence featuring a linear elastic orthotropic material model. Cohesive zone elements with the user defined material model presented in section 2 were used for the adhesive layer. The crack arresting features were modelled using fully integrated solid elements and a linear elastic isotropic material model. Figure 3 compares the numerical model to the micro-section of a hybrid adhesively bonded RNPJ. Contact and tied interfaces were defined as highlighted in Figure 3. A friction coefficient for composite-steel of 0.1 was selected according to [13]. Material data for the composite material and adhesive are presented in Table 1 and Table 2 respectively. In the absence of dedicated material tests related to the traction separation curve of the CZE some parameters are still assumed.

Excerpt from ISBN 978-3-00-053387-7

Furthermore, the Paris' Law curve has been experimentally characterized for only for a MMR, corresponding to the CLS-specimen. Equation 5 was then calibrated to fit the simulation to experimental results of the CLS-specimen with a RNPJ at 20kN load.

E_1	E_2, E_3	$\upsilon_{12}, \upsilon_{13}$	υ_{23}	G_{12}, G_{13}	G_{23}	t
$[MPa]$	$[MPa]$	–	–	$[MPa]$	$[MPa]$	$[mm]$
163000	96000	0.31	0.45	5400	4900	0.125

Table 1: Material properties of Hexply IM7/8552

K_I	K_{II}	t_I^0	t_{II}^0	G_{Ic}	G_{IIc}	$C_{1_{CLS}}$	$C_{2_{CLS}}$
$[N/mm^3]$	$[N/mm^3]$	$[MPa]$	$[MPa]$	$[N/mm]$	$[N/mm]$	$[mm/cyc]$	–
2800	1000	15	10	600	12000	0.00674	2.47

Table 2: Material properties of Scotch-Weld 9323 B/A

This paper aims to present the methodology of identifying and quantifying crack arresting mechanisms. The following parameters were therefore evaluated:

a) 1D crack growth: crack length a vs number of cycles N (experimentally and numerically)
b) 2D change of total strain energy release rate: $G_{tot} = G_I + G_{II}$ (numerically)
c) 2D change of mixed mode ratio: MMR (numerically)

where a 1D evaluation refers to measurements performed on the specimen sides as shown in Figure 4 and a 2D evaluation presents the spatial change of certain parameters. Once the crack passed through an element, values are stored so that the element loading during fatigue degradation can be compared at the end of the simulation in one plot. To reduce computational cost only the dashed area in Figure 4 is evaluated.

Figure 4: Definition of section to be evaluated during test and simulation (left); comparison of numerical and experimental crack shape (right)

Experimental results of crack growth are presented in Figure 5. They show a similar behavior for all joint configurations and load levels consisting of an initial constant crack growth rate followed by a transition zone in which the crack growth rate is continuously reduced. Comparing the RNPJ configuration at all load levels it is evident that even at very different initial crack growth rates $(da/dN)_{\text{ini}}$ the crack growth behavior and hence the crack arresting capability is almost identical. The Pin Configuration PC shows the least effective crack arrest. The crack growth reduction starts at a location further behind the fastener location and with a lower rate of change compared to the RNJP and BC. The crack growth of the bolt configuration BC lies in between the RNPJ and PC. Both the PC and BC show a re-acceleration of the crack after an initial crack growth reduction. For the PC this can be attributed to debonding of the pin previously attached to the retainer. It is believed that the cracking of the adhesive results from a significant bending moment on the pin. A similar behavior was not found in the RNPJ configuration as the bending moment is prohibited by the bolt and washers. For the BC no clear explanation could be found. While in the first specimen the bolt was installed to barely touch the surface, a slight tightening of 1.3Nm was used for the second specimen, which showed a delay of crack acceleration. Further investigations are planned to better understand this phenomenon.

Comparing experimental results to the numerical simulations shown in Figure 5 it can be found that simulations are able to closely predict the crack growth behavior for the RNPJ configuration at all three

Excerpt from ISBN 978-3-00-053387-7

load levels. This is supported by the good prediction of the two-dimensional crack shape shown in Figure 4. Furthermore, the fatigue simulations capture well crack growth in the transition zone of the PC. However, it has been observed that the results are very sensitive to the selected friction coefficient. The debonding of the pin was not identified by the simulation as corresponding interfaces were not previously defined. Finally, simulation of the BC predicts a crack growth reduction that is significantly faster than that observed during the experiment and re-acceleration is not captured. Understanding these differences is part of our ongoing research.

In order to understand the different crack arresting capabilities the influence of the three different joint configurations on loading at the adhesive is presented in Figure 6. Considering the changing MMR a very similar behavior can found for the RNPJ and BC. The PC also shows a changing MMR resulting from the friction at the pin hole interface but significantly delayed. On the other hand the pin continuously reinforces the structure resulting in a reduction of G_{tot} which is even more evident for the RNPJ; whereas the BC only slightly reduces the loading in the adhesive. Comparing the shape of the MMR equal to 1 for the RNPJ a strong correlation to the crack front shape can be found, supporting the assumption that the changing MMR is the leading crack arresting feature for the given joint. To achieve a fast and efficient crack arrest additional bearing load transfer is still required.

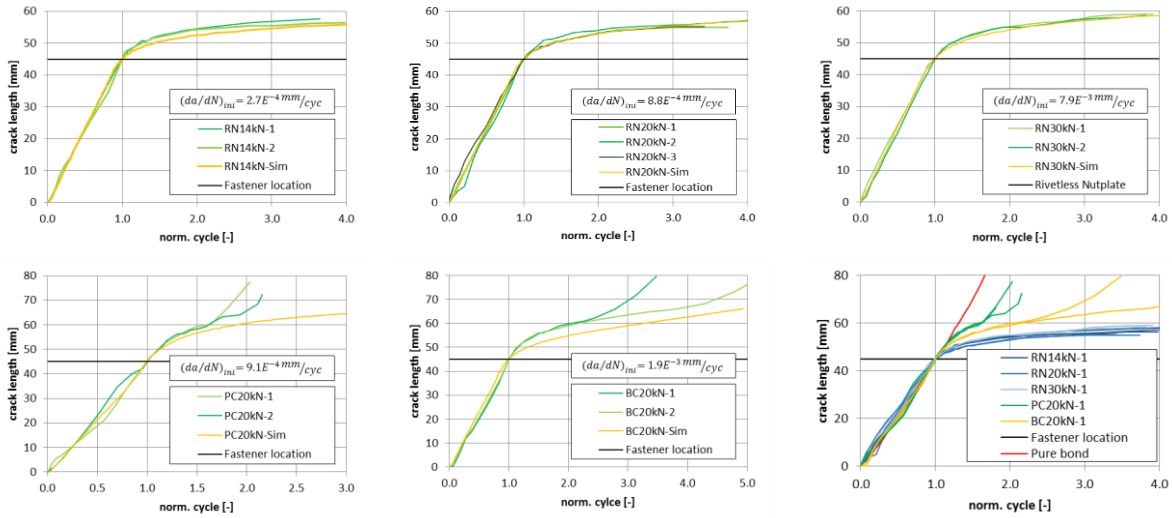

Figure 5: 1D experimental and numerical crack growth for different joint configurations (top left to bottom right): RNPJ @ 14kN; RNPJ @ 20kN, RNPJ @ 30kN; PC @ 20kN; BC @ 20kN; Comparison

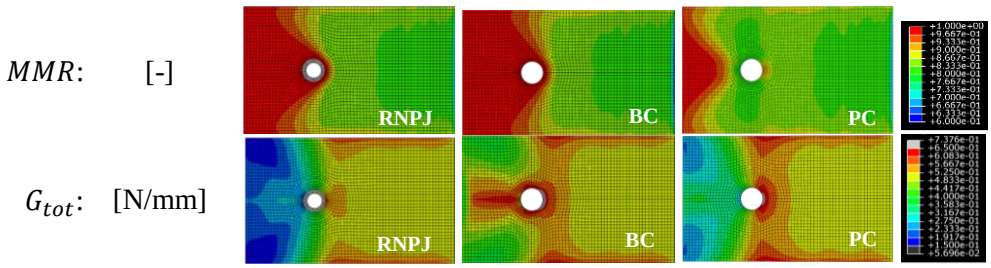

Figure 6: Crack arresting features a) rivetless nut plate joint b) numerical model of rivetless nut plate joint c) pin coniguration d) bolt configuration

5. Conclusions

The screening test results indicate excellent crack arresting capabilities of the rivetless nut plate in the adhesive bondline. The relative crack growth reduction is almost identical for all load levels investigated. Both pin and bolt configurations show a reduced and delayed crack arrest, while the bolt

Excerpt from ISBN 978-3-00-053387-7

configuration is superior to the pin configuration. In both cases a reacceleration of crack speed was observed. While this can be correlated to the debonding of the pin from the retainer no reason was so far identified for the bolt configuration. Numerical simulations of fatigue crack growth correlate very well for all rivetless nut plate joint configurations investigated and shows good results for the pin and bolt configuration while not all effects have yet been fully captured. Comparing crack growth to the change of mixed-mode ratio and total strain energy release rate for all configurations the reduction of mixed-mode ratio due to the fastener was identified as the leading crack arresting mechanism. The difference between the bolt configuration and the rivetless nut plate joint, however, shows that efficient crack arrest required further reinforcement through bearing load transfer.

Acknowledgments

The support of the European Union Seventh Framework Programme (FP7/2007-2013), under grant agreement n° 314180 (Project BOPACS: Boltless Assembling of Primary Aerospace Composite Structures) is gratefully acknowledged.

References

[1] Federal Aviation Administration, "AC 20-107B - Composite Aircraft Structures," 24 August 2010.

[2] Boltless assembling Of Primary Composite Structures (BOPACS), "Description of Work," EU FP7 Research Project, 2012.

[3] M. Wahab, "Fatigue in Adhesively Bonded Joints: A Review," *ISRN Materials Science,* vol. 2012, 2012.

[4] S. Stelzer, R. Jones and A. Brunner, "Interlaminar fatigue crack growth in carbon fiber reinforced composites," in *19th International Conference on Composite Materials*, Montréal, 2013.

[5] S. Azari, M. Papini, J. Schroeder and J. Spelt, "The effect of mode ratio and bond interface on the fatigue behavior of a highly-toughened epoxy," *Engineering Fracture Mechanics,* vol. 77, pp. 395-414, 2010.

[6] R. Sachse, P. A.K., W. Adebahr, M. Klein, M. Käß and P. Middendorf, "Experimental Investigation of Mechanical Fasteners Regarding their Influence on Crack Growth in Adhesively Bonded CFRP-Joints Subjected to Fatigue Loading," in *20th International Conference on Composite Materials,* Copenhagen, 2015.

[7] K. Y. Lin, L. Richard and W. Liu, "DELAMINATION ARREST FASTENERS IN AIRCRAFT COMPOSITE STRUCTURES," in *19th INTERNATIONAL CONFERENCE ON COMPOSITE MATERIALS* , Montréal, 2013.

[8] A. Turon, J. Costa, P. Camanho and C. Davila, "Simulation of delamination in composites under high-cycle fatigue," *Composites: Part A 38,* pp. 2270-2282, 2007.

[9] P. Harper and S. Hallett, "A fatigue degradation law for cohesive interface elements – Development and application to composite materials," *International Journal of Fatigue 32* , pp. 1774-1787, 2010.

[10] L. Kawashita and S. Hallett, "A crack tip tracking algorithm for cohesive interface element analysis of fatigue delamination propagation in composite materials," *International Journal of Solids and Structures 49* , pp. 2898-2913, 2012.

[11] R. Sachse, A. K. Pickett, M. Käß and P. Middendorf, "Numerical Simulation of Fatigue Crack Growth in the Adhesive Bondline of Hybrid CFRP Joints," in *Composites 2015,* Bristol, 2015.

[12] "Cherry Aerospace," 6 10 2014. [Online]. Available: http://cherryaerospace.com/.

[13] C. Friedrich and H. Hubbertz, "Friction behavior and preload relaxation of fastening systems," *Composite Structures 110* , p. 335–341, 2014.

Excerpt from ISBN 978-3-00-053387-7